The Mixed Spin-1 and Spin-5/2 BEG Model in a Staggered Magnetic Field

Joël Kplé[a], Rachidi Adeniyi Yessoufou[a] and Félix Hontinfinde[a,b,1]
[a] *Département de Physique (FAST) et Institut des Mathématiques et de Sciences Physiques (IMSP), Université d'Abomey-Calavi, Porto-Novo, Benin*
[b] *The Abdus Salam International Centre for Theoretical Physics, Trieste, Italy*

The mixed spin-1 and spin-$\frac{5}{2}$ Ising model with bilinear (J) and biquadratic (K) nearest-neighbor exchange interactions and a single-ion potential or crystal-field interaction (D) is investigated by means of recursion relations on the Bethe lattice in the presence of a staggered magnetic field. The interactions are assumed to be only between nearest-neighbors. The competition between model parameters leads to very rich T=0 phase diagrams which may be useful to explore interesting domains of the finite-temperature phase diagrams of the model. Some thermal properties of the system are presented. The magnetization is also described by numerical simulations of the model on a square lattice using Glauber stochastic dynamics in the presence of an oscillating external staggered field. Our present results bear little resemblance to those previously reported on various kinetic Ising systems obtained by integrating differential equations.

1. Introduction

In recent years, mixed spin systems of different magnitudes, in particular, mixed (1/2,5/2) [1–3], (3/2,5/2) [4–8], (1,2) [9–11] Ising models have been more or less studied in condensed matter and statistical physics to describe a variety of multicritical (order-disorder) phenomena often observed in real objects. Indeed, these systems become relevant to an investigation of new bimetallic molecular compounds, the structure of which bears some resemblance with two magnetic atoms alternating on a regular lattice [12]. Numerous experiments indicate that a mix of 3/2 and 5/2 spins may show the unusual magnetic properties of certain types of ferric heme proteins known as ferricitochrom [13]. On the other hand, many potential applications use molecular-based materials, where ferrimagnetic ordering or compensation points play an essential role [14]. The mixed (1,5/2) Ising model is an interesting case that remains however less studied in the literature and calls for a deeper investigation. Recently, this model has been proposed by Yessoufou et al. [15] and studied by means of recursion relations. They obtained fairly rich set of critical behaviors in the presence as well as in the absence of an external static magnetic field. In this paper, we extend this model by considering a staggered magnetic field. The motivation comes from several recent works, which pointed out the importance of this particular constraint in genesis of anomalous static and dynamic magnetic properties in one-dimensional spin chains [16]. We draw a deep analysis of the ground states (GS) configurations of the model. The results may be useful to explore interesting regions of the finite-temperature phase diagrams. Similar attempts have been made in the literature to investigate the ground states of various Ising systems and the reported results have been used by other researchers (see [17] and references therein). Most thermal transitions observed in the model are associated with the magnetization reversal phenomenon and are of first order. Kinetic Monte Carlo (KMC) simulations with the Bortz, Kalos and Lebowitz (BKL) [18] algorithm and Glauber dynamics [19] are considered on a square lattice with periodic boundary conditions to check some results obtained by recursion relations and explore the dynamical behavior of the lattice magnetization in the presence of a time-dependent sinusoidal staggered field. In this investigation, transition probabilities when the system runs from one configuration to another are not constant as considered in some previous works [20], but depend on the change in the system's energy at any stage of the simulation process. Our calculation shows that stationary values of the lattice magnetization behave in a non-trivial way with the field frequency and amplitude. Such a result somewhat contrasts with those reported on several Ising

[1] fhontinfinde@yahoo.fr

systems by integrating kinetic equations [20, 21].

In Section 2, we describe the model and derive the recursion relations. In Section 3, we construct and comment on different T=0 phase diagrams. Some insight on the finite temperature phase diagrams is given in Section 4. In Section 5, we describe the BKL simulation algorithm. In Section 6, simulation results are presented for a sinusoidal external field. The last section is devoted to conclusions.

2. The Recursion Relations of the Model

2.1. The BEG model Hamiltonian

The model is defined on the Bethe lattice (Fig. 1), which consists of two different types of magnetic atoms A and B with spin variables S_i and σ_j. The interaction Hamiltonian considered is that of Blume-Emery-Griffiths (BEG) type [22] and is written in the form (see [15]):

$$H = -J\sum_{\langle ij\rangle} S_i\sigma_j - K\sum_{\langle ij\rangle} S_i^2\sigma_j^2 - D\Big(\sum_i S_i^2 + \sum_j \sigma_j^2\Big) - h_1\sum_i S_i - h_2\sum_j \sigma_j \tag{1}$$

Where, $\langle ij\rangle$ indicates a pair of nearest-neighboring sites; J and K are coupling constants. The first sum runs over nearest-neighbor sites. The second term denotes the biquadratic isotropic exchange interactions, which should be considered for a high-spin system ($S \geq 1$) [23]. Adler gave a discussion of this term through an extensive review [24] of experimental results establishing its importance in a variety of compounds. The third term is a single ion anisotropy energy due to crystalline field. h_1 and h_2 are the external staggered fields acting on the spins. Originally, this Hamiltonian has been introduced to describe the thermodynamical properties of $He^3 - He^4$ mixtures [22].

2.2. The recursion relations

The Bethe lattice consists of a central spin S_0 which may be called the first generation spin. S_0 has a number q of nearest-neighbors, which form the second generation spins. Each site of this generation is joined to $q-1$ nearest-neighbors. Thus, the second generation has $q(q-1)$ nearest-neighbors which form the third generation and so on to infinity as shown in Fig 1.

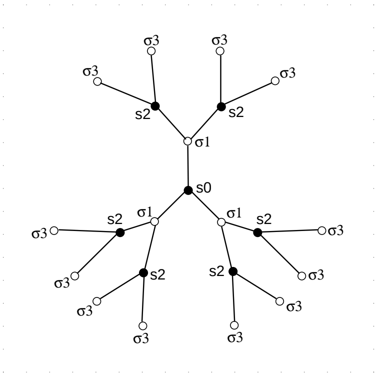

FIG. 1: A Bethe lattice of coordination number $q = 3$ consisting of two different types of atoms A ans B with spin variables S and σ respectively.

The partition function of the model is given by:

$$Z = \sum e^{-\beta H} = \sum_{Spc} P(Spc)$$

Where, $P(Spc)$ can be thought of as an non-normalized probability distribution over the spin configuration, Spc (e.g., S, σ). S_i and σ_j indicate the spins' values at sites i and j, respectively. If the Bethe lattice is cut at some central point with a spin S_0, spin of type 1, then it splits up into q identical branches. Each of these q disconnected pieces is a rooted tree at a central spin S_0. This implies that $P(S_0)$, i.e., $Spc = S_0$, of a spin configuration with the spin value S_0 at the central site, can be written as:

$$P(S_0) = \exp\Big[\beta(DS_0^2 + h_1S_0)\Big]\Big[g_n(S_0)\Big]^q \tag{2}$$

$$P(\sigma_1) = \exp\Big[\beta(D\sigma_1^2 + h_2\sigma_1)\Big]\Big[g_{n-1}(\sigma_1)\Big]^q \tag{3}$$

Where, S_0 is the central spin value of the lattice, $g_n(S_0)$ the partition function of an individual branch and the suffix n represents the fact that the sub-tree has n shells, i.e., n steps from the root to the boundary sites. Therefore, $g_n(S_0)$ is written in terms of summation over spin set $\{\sigma_1\}$ as

$$g_n(S_0) = \sum_{\{\sigma_1\}} \exp\Big[\beta(JS_0\sigma_1 + D\sigma_1^2 + KS_0^2\sigma_1^2 + h_2\sigma_1)\Big]\Big[g_{n-1}(\sigma_1)\Big]^{q-1} \tag{4}$$

Advancing along any branch, we get a site that is next-nearest to the central spin, hence $g_{n-1}(\sigma_1)$ is expressed as follows [15]:

$$g_{n-1}(\sigma_1) = \sum_{\{S_2\}} \exp\Big[\beta(JS_2\sigma_1 + DS_2^2 + KS_2^2\sigma_1^2 + h_1S_2)\Big]\Big[g_{n-2}(S_2)\Big]^{q-1} \qquad (5)$$

In order to find the recursion relations, we introduce the following variables as a ratio of g_n functions for the spin-1 as follows:

$$X_n = \frac{g_n(+1)}{g_n(0)}, \quad Y_n = \frac{g_n(-1)}{g_n(0)} \qquad (6)$$

and for the spin-5/2 as the ratio of g_{n-1} functions

$$A_{n-1} = \frac{g_{n-1}(5/2)}{g_{n-1}(-1/2)}, \quad B_{n-1} = \frac{g_{n-1}(-5/2)}{g_{n-1}(-1/2)},$$

$$C_{n-1} = \frac{g_{n-1}(3/2)}{g_{n-1}(-1/2)} \qquad (7)$$

$$D_{n-1} = \frac{g_{n-1}(-3/2)}{g_{n-1}(-1/2)}, \quad E_{n-1} = \frac{g_{n-1}(1/2)}{g_{n-1}(-1/2)} \qquad (8)$$

The BEG model is characterized by two order parameters, the magnetization M and the quadrupolar moment Q. Four order parameters: $M_{A,B}$ and $q_{A,B}$, where A, B refer to the two sublattices may be considered. Their expressions follow:

$$M_A = Z_1^{-1}\sum_{\{S_0\}} S_0P(S_0), \quad q_A = Z_1^{-1}\sum_{\{S_0\}} S_0^2P(S_0) \qquad (9)$$

they are easily expressed in terms of the recursion relations, namely Eqn. (6), and calculated as:

$$M_A = \frac{e^{(\beta D)}(e^{(\beta h_1)}X_n^q - e^{(-\beta h_1)}Y_n^q)}{1 + e^{(\beta D)}(e^{(\beta h_1)}X_n^q + e^{(-\beta h_1)}Y_n^q)} \qquad (10)$$

$$q_A = \frac{e^{(\beta D)}(e^{(\beta h_1)}X_n^q + e^{(-\beta h_1)}Y_n^q)}{1 + e^{(\beta D)}(e^{(\beta h_1)}X_n^q + e^{(-\beta h_1)}Y_n^q)} \qquad (11)$$

Similarly, we get:

$$M_B = \frac{\Big\{5e^{(6\beta D)}(e^{(3\beta h_2)}A_{n-1}^q - e^{(-2\beta h_2)}B_{n-1}^q) + 3e^{(2\beta D)}(e^{(2\beta h_2)}C_{n-1}^q - e^{(-\beta h_2)}D_{n-1}^q) + (e^{(\beta h_2)}E_{n-1}^q - 1)\Big\}}{\Big\{2e^{(6\beta D)}(e^{(3\beta h_2)}A_{n-1}^q + e^{(-2\beta h_2)}B_{n-1}^q) + 2e^{(2\beta D)}(e^{(2\beta h_2)}C_{n-1}^q + e^{(-\beta h_2)}D_{n-1}^q) + 2(e^{(\beta h_2)}E_{n-1}^q + 1)\Big\}} \qquad (12)$$

$$q_B = \frac{\Big\{25e^{(6\beta D)}(e^{(3\beta h_2)}A_{n-1}^q + e^{(-2\beta h_2)}B_{n-1}^q) + 9e^{(2\beta D)}(e^{(2\beta h_2)}C_{n-1}^q + e^{(-\beta h_2)}D_{n-1}^q) + (e^{(\beta h_2)}E_{n-1}^q + 1)\Big\}}{\Big\{4e^{(6\beta D)}(e^{(3\beta h_2)}A_{n-1}^q + e^{(-2\beta h_2)}B_{n-1}^q) + 4e^{(2\beta D)}(e^{(2\beta h_2)}C_{n-1}^q + e^{(-\beta h_2)}D_{n-1}^q) + 4(e^{(\beta h_2)}E_{n-1}^q + 1)\Big\}} \qquad (13)$$

First-order phase transitions in the model may be detected using either the analysis of the free energy of the system or jumps in the total magnetizations. The second order transitions are obtained when both sublattice magnetizations continuously vanish (see [15]).

3. T=0 Phase Diagrams

The staggered magnetic field is obtained by setting h=h_1=-h_2. The GS energies are obtained from equation (1) in units of $|J|$ by rewriting it in the following form,

$$\frac{E}{|J|} = -\sum_{\langle ij\rangle}\Big[\frac{J}{|J|}S_i\sigma_j + \frac{D}{q|J|}(S_i^2+\sigma_j^2) + \frac{K}{|J|}S_i^2\sigma_j^2 + \frac{h}{q|J|}(S_i-\sigma_j)\Big] \qquad (14)$$

Where, the summation runs over all nearest-neighbor sites.

We compare computed energy values of different spin configurations. Configurations with lowest energies for varying values of model parameters correspond to the GS configurations. The set of points in the parameters' space for which a given configuration is the ground state gives the stability region of this phase. It should be mentionned that the variable q is somewhat used as a hidden variable in the above definition of GS energies, therefore, these GS phase diagrams are obtained for a general q value, i.e., for any coordination number. In the diagrams, there are boundary lines (coexistence lines) separating different types of phases. The points at which these lines meet are multiphase points where all the involved phases coexist.

The GS phase diagrams are first constructed for fixed values of $h/q|J|$ in the plane $(D/q|J|, K/|J|)$. We first set $h/q|J| = 0$; the system becomes then invariant under a global inversion of spins. We compare the diagrams for positive and negative values of J and get results that are topologically independent of the sign of J with some common phases as (0,-1/2); (0,-5/2). The corresponding GS and energies are given in Table I. Equations of coexistence lines between phases are given in Table II. For $J < 0$, other phases of the diagram correspond to sublattices with antiparallel spins. For $J > 0$ and positive (non-zero) values of h/qJ, the energetically unfavorable phase (0,-3/2) appears and its domain grows while domains of other phases, namely (-1,-3/2),(1,1/2), (0,-1/2) and (0,-5/2) shrink. The partially ordered phases (0,-1/2) and (0, -5/2) recorded at h=0 are not stable at finite temperature in the absence of the field constraint [15]. We also notice that large values of D/qJ and K/J do not influence significantly the phase diagrams. The diagrams appear richer for small values of K/J with small and negative values of D/qJ. In the following, we will concentrate our investigation on this region of model parameters at relatively small values of h/qJ. In regions IV and V, the energies of the ground states are independent of the sign of J. At the diagram's points $(\frac{D}{q|J|}, \frac{K}{|J|}) = (-\frac{5}{4}, 1)$, $(\frac{5}{28}, -\frac{3}{7})$, $(\frac{1}{14}, -\frac{4}{7})$, $(0, -2)$, $(-\frac{1}{2}, 0)$, three different regions coexist.

In the following, we first consider the model with ferromagnetic coupling $J > 0$ and positive values of h/qJ. For negative values of h/qJ, the magnetizations only change sign due to the symmetry requirement, $M(-h) = -M(h)$ as observed in Table III, where nine possible spin configurations are recorded with their respective energies.

The GS phase diagrams in the $(D/qJ, K/J)$ plane for different values of h/qJ are shown in Fig. 2b-f. The topology of these diagrams is somewhat similar to the one obtained for $h/qJ = 0$. It is important to mention that phase (IX) only prevails in the negative part of the D/qJ-axis.

TABLE I: Ground state energies of the model for $h = 0$; $D' = D/q|J|$, $K' = K/|J|$ (Fig. 2a).

Phase	Ground state				Energy
I	$(\pm1, \pm5/2)$	$J>0$	$(\pm1, \mp5/2)$	$J<0$	$-\frac{5}{2} - \frac{29}{4}D' - \frac{25}{4}K'$
II	$(\pm1, \pm3/2)$	$J>0$	$(\pm1, \mp3/2)$	$J<0$	$-\frac{3}{2} - \frac{13}{4}D' - \frac{9}{4}K'$
III	$(\pm1, \pm1/2)$	$J>0$	$(\pm1, \mp1/2)$	$J<0$	$-\frac{1}{2} - \frac{5}{4}D' - \frac{1}{4}K'$
IV		$(0, \pm5/2)$			$-\frac{25}{4}D'$
V		$(0, \pm1/2)$			$-\frac{1}{4}D'$

TABLE II: Coexistence curves of the model for $h = 0$; $D' = D/q|J|$, $K' = K/|J|$. Different phases are defined in Table I.

Region	Coexistence line	D' Range	K' Range
I-II	$D' = -K' - \frac{1}{4}$	$-\frac{5}{4} \leq D' \leq \frac{5}{28}$	$-\frac{3}{7} \leq K' \leq 1$
I-IV	$D' = -25K' - \frac{5}{2}$	$D' \geq \frac{5}{28}$	$K' \leq -\frac{3}{7}$
I-V	$D' = -\frac{25}{28}K' - \frac{5}{14}$	$D' \leq -\frac{5}{4}$	$K' \geq 1$
II-III	$D' = -K' - \frac{1}{2}$	$-\frac{1}{2} \leq D' \leq \frac{1}{14}$	$-\frac{4}{7} \leq K' \leq 0$
II-IV	$D' = \frac{3}{4}K' + \frac{1}{2}$	$\frac{1}{14} \leq D' \leq \frac{5}{28}$	$-\frac{4}{7} \leq K' \leq -\frac{3}{7}$
II-V	$D' = -\frac{3}{4}K' - \frac{1}{2}$	$-\frac{5}{4} \leq D' \leq -\frac{1}{2}$	$0 \leq K' \leq 1$
III-IV	$D' = \frac{1}{20}K' + \frac{1}{10}$	$0 \leq D' \leq \frac{1}{14}$	$-2 \leq K' \leq -\frac{4}{7}$
III-V	$D' = -\frac{1}{4}K' - \frac{1}{2}$	$-\frac{1}{2} \leq D' \leq 0$	$-2 \leq K' \leq 0$
IV-V	$D' = 0$	$D' = 0$	$K' \leq -2$

For $0 < h/qJ < 1$, the ground state phase diagrams (see Fig. 2b,c) exhibit only six GS configurations, namely phases (I), (V), (VI), (VII), (VIII) and (IX). The phase (V) is present for all values of D/qJ. Positive K/J values enlarge its stability domain. On the other hand, as h/qJ increases, the phase (VIII) becomes more favorable and phases (I) and (VI) can only occur in some small restricted area. Note also that as h/qJ increases, the area of the phase (IX) is reduced, whereas areas of phases (VII) and (VIII) are extended.

For $h/qJ = 1$ (Fig. 2d), phases (I) and (VI) disappear and are replaced by two other phases when $1 < h/qJ < 3/2$, so that the number of phases becomes six as before. Here, phase I is replaced by phase IV. For $h/Jq = 3/2$ (Fig. 2e), phases (IV), (V), (VII), (VIII) and (IX) are observed. Phase (VI) which appears for previous values of h/qJ does not exist. For $3/2 < h/qJ < 5/2$, phases (IV), (V), (VII), (VIII), and (IX) remain in the same region as before, but phase (VI) is replaced by phase (III) for all $h/qJ > 3/2$.

At $h/qJ = 2.0$, the ground state phase diagram shows five visible configurations, i.e., phases (IV), (V), (VII), (VIII) and (IX); but the phase (III) also exists and lies along the multiphase line separating phases (IV), (V) and (IX). It appears evident that for larger values of h/qJ, $h/qJ = 5/2$ for instance, the phase (III) will be contained in a region separating phases (IV), (V) and (IX).

When $h/qJ = 5/2$, Fig. 2f, phases (II) and (V) coexist but for $h/qJ > 5/2$, this coexistence disappears and only phase (II) survives. According to their location in the GS phase diagrams, phases (II), (III) and (IV) appear as the result of a competition between the interaction parameters J and h.

The GS phase diagrams in Fig. 3 are obtained in the $(h/qJ, K/J)$ plane for some selected values of D/qJ. For positive and non-zero values of D/qJ, the system only presents configurations (II), (V) and (VII) as observed in Fig. 3a. The diagrams look similar for all positive values of the reduced crystal-field, which means that the latter has no splitting effect on the topology when its value remains in this range. At large values of K/J, phases (II) and (V) are separated by a multiphase line, but for lower negative values of K/J, phase (VII) is separated from phases (II) and (V) by two multiphase lines, the first one for $h/qJ > 5/2$ and the second one for $h/qJ < 5/2$. As K/J becomes more and more negative, the zero value of the spin becomes persistent, thus leaving the sublattice A in a diamagnetic zero phase. For

TABLE III: Ground states energies of the model for $J > 0$, and $h \neq 0$; $D' = D/qJ$, $K' = K/J$ and $h' = h/qJ$.

Phase	Ground state				Energy
I	$(+1,+1/2)$	$h' > 0$	$(-1,-1/2)$	$h' < 0$	$\begin{cases} -\frac{1}{2} - \frac{5}{4}D' - \frac{1}{4}K' - \frac{1}{2}h' & \text{si } h' > 0 \\ -\frac{1}{2} - \frac{5}{4}D' - \frac{1}{4}K' + \frac{1}{2}h' & \text{si } h' < 0 \end{cases}$
II	$(+1,-5/2)$	$h' > 0$	$(-1,+5/2)$	$h' < 0$	$\begin{cases} \frac{5}{2} - \frac{29}{4}D' - \frac{25}{4}K' - \frac{7}{2}h' & \text{si } h' > 0 \\ \frac{5}{2} - \frac{29}{4}D' - \frac{25}{4}K' + \frac{7}{2}h' & \text{si } h' < 0 \end{cases}$
III	$(+1,-3/2)$	$h' > 0$	$(-1,+3/2)$	$h' < 0$	$\begin{cases} \frac{3}{2} - \frac{13}{4}D' - \frac{9}{4}K' - \frac{5}{2}h' & \text{si } h' > 0 \\ \frac{3}{2} - \frac{13}{4}D' - \frac{9}{4}K' + \frac{5}{2}h' & \text{si } h' < 0 \end{cases}$
IV	$(+1,-1/2)$	$h' > 0$	$(-1,+1/2)$	$h' < 0$	$\begin{cases} \frac{1}{2} - \frac{5}{4}D' - \frac{1}{4}K' - \frac{3}{2}h' & \text{si } h' > 0 \\ \frac{1}{2} - \frac{5}{4}D' - \frac{1}{4}K' + \frac{3}{2}h' & \text{si } h' < 0 \end{cases}$
V	$(-1,-5/2)$	$h' > 0$	$(+1,+5/2)$	$h' < 0$	$\begin{cases} -\frac{5}{2} - \frac{29}{4}D' - \frac{25}{4}K' - \frac{3}{2}h' & \text{si } h' > 0 \\ -\frac{5}{2} - \frac{29}{4}D' - \frac{25}{4}K' + \frac{3}{2}h' & \text{si } h' < 0 \end{cases}$
VI	$(-1,-3/2)$	$h' > 0$	$(+1,+3/2)$	$h' < 0$	$\begin{cases} -\frac{3}{2} - \frac{13}{4}D' - \frac{9}{4}K' - \frac{1}{2}h' & \text{si } h' > 0 \\ -\frac{3}{2} - \frac{13}{4}D' - \frac{9}{4}K' + \frac{1}{2}h' & \text{si } h' < 0 \end{cases}$
VII	$(0,-5/2)$	$h' > 0$	$(0,+5/2)$	$h' < 0$	$\begin{cases} -\frac{29}{4}D' - \frac{5}{2}h' & \text{si } h' > 0 \\ -\frac{29}{4}D' + \frac{5}{2}h' & \text{si } h' < 0 \end{cases}$
VIII	$(0,-3/2)$	$h' > 0$	$(0,+3/2)$	$h' < 0$	$\begin{cases} -\frac{9}{4}D' - \frac{3}{2}h' & \text{si } h' > 0 \\ -\frac{9}{4}D' + \frac{3}{2}h' & \text{si } h' < 0 \end{cases}$
IX	$(0,-1/2)$	$h' > 0$	$(0,+1/2)$	$h' < 0$	$\begin{cases} -\frac{1}{4}D' - \frac{1}{2}h' & \text{si } h' > 0 \\ -\frac{1}{4}D' + \frac{1}{2}h' & \text{si } h' < 0 \end{cases}$

$D/qJ \leq 0$ (Fig. 3c,d), the GS phase diagrams deeply change and present a particular richness. Multiphase lines are splitted by new configurations. For example, for $D/qJ = 0$ (Fig. 3b), the configurations (I) and (VI) are observed in addition to other three configurations; the equations of coexistence lines are given in Table IV. At the points $(\frac{h}{qJ} = \frac{3}{16}, \frac{K}{J} = -\frac{1}{2})$, $(\frac{h}{qJ} = \frac{5}{2}, \frac{K}{J} = 0)$ and $(\frac{h}{qJ} = \frac{15}{41}, \frac{K}{J} = -\frac{14}{41})$, three phases coexist.

The GS phase diagrams in the $(h/qJ, D/qJ)$ plane are displayed in Fig. 4. For $K/J > 0$ (Fig. 4a,b) phases (II), (III), (IV), (V) and (IX) are still present and the two panels look similar. For $K/J = 0$ (Fig. 4c), the equations of coexistence lines are given in Table V. From this diagram, one can deduce some interesting features: there are two points where three phases coexist; $(\frac{h}{qJ} = \frac{5}{2}, \frac{D}{qJ} = 0)$ and $(\frac{h}{qJ} = 3, \frac{D}{qJ} = -\frac{1}{2})$, and two points where four phases coexist: $(\frac{h}{qJ} = 1, \frac{D}{qJ} = -\frac{1}{2})$ and $(\frac{h}{qJ} = 2, \frac{D}{qJ} = -\frac{1}{2})$.

When $K/J < 0$, the multiphase lines split again by new configurations (Fig. 4d-f). The GS phase diagrams show a vast variety of ground states for selected negative values of (K/J). They look qualitatively similar.

Some results in the case $J < 0$ are illustrated in Fig. 5. Six different types of GS configurations are found (see Table VI), namely phases (II), (III), (IV), (VII), (VIII) and (IX). In Fig. 5, we construct the GS phase diagrams on the $(h/q|J|, K/|J|)$ plane for some values of $D/q|J|$. For $D/q|J| = 1.0$ (Fig. 5a) only phases (II) and

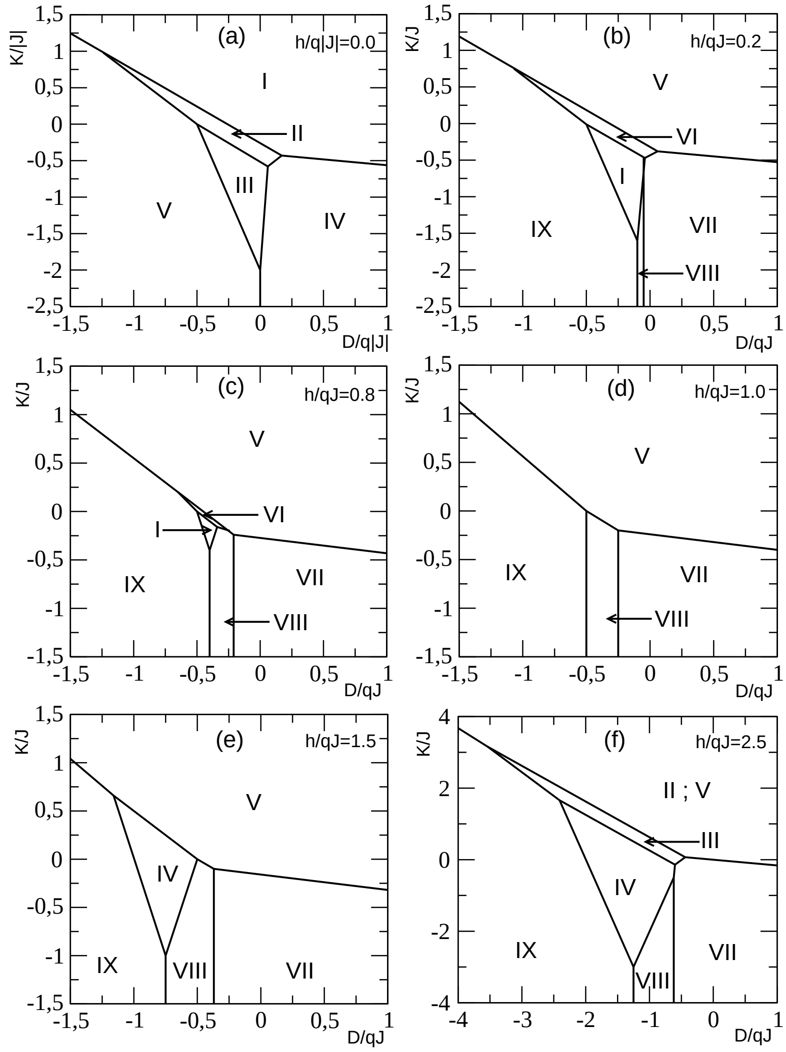

FIG. 2: Ground state phase diagrams for selected values of h/qJ and varying D/qJ and K/J. The different phases indicated with roman numbers are explicited in Table I for $h = 0$ (panel a) and in Table III for non-zero h/qJ (panels b-f).

(VII) are recovered with (II) in the upper half plane, while the other is contained in the lower half plane. When $D/q|J| = 0.0$ (Fig. 5b), two additional configurations (III and IV) appeared. The equation of coexistence lines are given in Table VII. Fig.5c is obtained for $D/q|J| = -0.50$, where new phases appeared in addition to other four phases. The GS phase diagram in Fig. 5d is similar to that in Fig. 5c but now, a boundary between phases (III) and (IX) is observed.

We have also calculated GS phase diagrams in the $(h/q|J|, D/q|J|)$ plane for selected values of $K/|J|$. They appear less rich and complicated than those obtained for $J > 0$. For $K/|J| = 1.0$, only phases (II), (III), (IV) and (IX) are observed. At $K/|J| = 0.0$, the phase diagram looks similar to the previous one except that the boundary between phases (III) and (IX) disappears. The equations of coexistence lines are given in Table VIII and the indicated phases are explained in Table VI.

4. Thermal Phase Diagram of the Model

Beyond the T=0 phase diagram, one would like to know the systems behavior when the temperature is raised from zero to higher values. Some results to deal with this concern are displayed through Fig. 6. In the following, we take $J > 0$ and q=3. In Fig. 6a, all other couplings are zeroed. One observes that the sub-lattice magnetizations decreases from their T=0 saturation values to zero continuously, whereas the associated quadrupole moments still have non-zero values. The transition to the disordered paramagnetic phase is clearly of second order. In the paramagnetic phase, several anti-parallel spins may exist due to the non-zero values of q_A and q_B. The influence of h on the previous results is presented in Fig. 6b, where $h/J = 0.2$. The behavior of Magnetization shows agreement with Fig. 2b. Indeed, Fig. 6b shows a T=0 saturation phase, which is (-1,-5/2), i.e., phase V in Table III. When $D/qJ = 0$ and $K/J = 0$, we get exactly the phase V as predicted in Fig. 2b. There, one easily identifies two jumps in m_A and m_B corresponding to first order transitions between stable ordered phases. The order parameters q_A and q_B seem not to be affected by these transitions. This suggests that these transitions are simply associated to a global magnetization reversal of the system. It is clear that a second order transiton is absent here. Depending on the field strength, the magnetization reversal occur in Ising systems either by nucleation of a single critical droplet (of spins) of the new phase or by simultaneous nucleation of many critical droplets [25]. The paramagnetic phase is reached at high temperature through a crossover region.

In Fig. 6c-f some thermal phase diagrams are presented for some selected values of D/J and K/J. One observes that positive values of K/J or D/J lead to some reentrant phase diagrams with about two first-order transition temperature values T_{c1} and T_{c2} at fixed h/J and varying T/J. T_{c1} disappears with decreasing K/J and also D/J as in Fig. 6d. Concerning the transitions, they are of two kinds: magnetization reversal and low-spin to high-spin kind similar to the one often observed in spin-crossover solids [26]. In the latter case, subsequent jumps may be observed in the quadrupole moments of the system. In Fig. 6f, we compare order-disorder effect of coupling constants D and K on the model. When both are non-zero with positive values, results are similar to the case $D/J = 0$ and $K/J = 0.5$; this means that in the presence of K/J and h/J, the coupling D/J is actually playing a minor role in the spin-flip dynamics. One can also notice that positive values of D and K have a stabilizing effect on the T=0 phases at low temperature (see Fig. 6c,e).

Other phases from Table III are found at other values of model parameters. For example, at $D/J = -1$ and $K/J = -1$ (see Fig. 4f), phase (0,-1/2) prevails at $h/J = 0.1$ and low values of T/J (phase IX in Table III) and decays as T increases to (0,0). At $h/J = 1$, the T=0 saturation phase is (1,1/2), which transits to phase (0,-1/2) and later to the paramagnetic phase (0,0). At $h/J = 1.5$, we gets at low T, phase (1,1/2) which transits to phase (0,-3/2) and later decays to phase (0,0) at high temperature. At $h/J = 5/2$, the T=0 saturation phase is (0,-3/2); it also decays to (0,0). The high-temperature phase is always the paramagnetic phase (0,0). It is reached through second order transitions at $h/J = 0$ for all model parameters considered in the text.

5. KMC Simulation Procedure

Monte Carlo simulations are numerical experiments that have been proven efficient in studying a wide variety of physical systems ranging from elementary particle systems to those in astronomy (see [27] and references therein). Here, we use the algorithm developed by BKL [18] to investigate some dynamical properties of the model on a square lattice of size L with the coordination number $q = 4$. The simulation is propagated as follows. First, an initial configuration $\overline{\sigma}$ (of linear size L) of the system is chosen and then one calculates the total number of possible spin-flip processes. This leads to another configuration $\overline{\sigma'}$, say N. Let us denote by $W(\overline{\sigma} \to \overline{\sigma'})$ the transition probability from $\overline{\sigma}$ to $\overline{\sigma'}$. By using the Glauber spin-flip dynamics, W reads [19]:

$$W(\overline{\sigma}, \overline{\sigma'}) = \frac{1}{1 + e^{\beta \Delta E}} \tag{15}$$

Where, ΔE denotes the change in the energy of the system associated to the spin-flip move. Then, one calculates the total evolution rate $R(\overline{\sigma})$ of $\overline{\sigma}$ by considering all possible processes:

$$R(\overline{\sigma}) = \sum_{a=1}^{N} W_a \tag{16}$$

Where, a stands for the number of possible spin-flip process. After that, two random numbers

$0 \leq r_1, r_2 \leq 1$ are chosen to calculate the real lifetime $\tau(\overline{\sigma}) = -\ln(r_1)/R(\overline{\sigma})$ of configuration $\overline{\sigma}$ and a random evolution rate: $\eta(\overline{\sigma}) = r_2 R(\overline{\sigma})$. The number of processes is b such that the partial sum:

$$\sum_{a=1}^{b} W_a > \eta(\overline{\sigma}) \tag{17}$$

is realized with probability 1. After a suitable number n_{MC} (found to be about $4.10^3 L^2$ up to L=100) of spin updates, the steady state is reached. The total evolution time $\overline{t}$ is given by: $\overline{t} = \sum_{\overline{\sigma}} \tau(\overline{\sigma})$, where the sum runs over all spin configurations generated up to the steady state. Different physical quantities (e.g., magnetization m, fourth order cumulant U and others) are calculated by a time-averaging procedure. The calculated fourth order cumulant has the expression: $U = 1 - \frac{<m^4>}{3<m^2>^2}$.

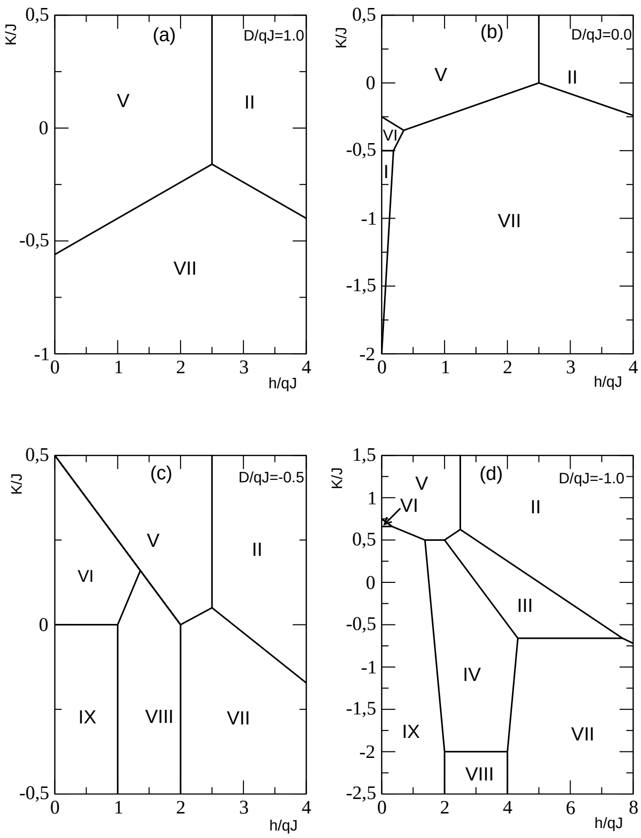

FIG. 3: Ground state phase diagrams for selected values of D/qJ and varying h/qJ and K/J. The different phases indicated by Roman numbers are explained in Table III.

TABLE IV: Coexistence curves of the model for $D = 0$; $K' = K/J$ and $h' = h/qJ$. Different phases refer to Table III.

Region	Coexistence line	K' Range	h' Range
I-VI	$K' = -\frac{1}{2}$	$K' = -\frac{1}{2}$	$0 \leq h' \leq \frac{3}{16}$
I-VII	$K' = 8h' - 2$	$-2 \leq K' \leq -\frac{1}{2}$	$0 \leq h' \leq \frac{3}{16}$
II-V	$h' = \frac{5}{2}$	$K' \geq 0$	$h' = \frac{5}{2}$
II-VII	$K' = -\frac{4}{25}h' + \frac{2}{5}$	$K' \leq 0$	$h' \geq \frac{5}{2}$
V-VI	$K' = -\frac{1}{4}h' - \frac{1}{4}$	$-\frac{14}{41} \leq K' \leq -\frac{1}{4}$	$\frac{3}{16} \leq h' \leq \frac{15}{41}$
V-VII	$K' = \frac{4}{25}h' - \frac{2}{5}$	$-\frac{14}{41} \leq K' \leq 0$	$\frac{15}{41} \leq h' \leq \frac{5}{2}$
VI-VII	$K' = \frac{8}{9}h' - \frac{2}{3}$	$-\frac{1}{2} \leq K' \leq -\frac{14}{41}$	$\frac{3}{16} \leq h' \leq \frac{15}{41}$

TABLE V: Coexistence curves of the model for $K = 0$; $D' = D/qJ$ and $h' = h/qJ$. Different phases refer to Table III.

Region	Coexistence line	D' Range	h' Range
II-III	$D' = -\frac{1}{4}h' + \frac{1}{4}$	$D' \leq -\frac{1}{2}$	$h' \geq 3$
II-V	$h' = \frac{5}{2}$	$D' \geq 0$	$h' = \frac{5}{2}$
II-VII	$D' = -h' + \frac{5}{2}$	$-\frac{1}{2} \leq D' \leq 0$	$\frac{5}{2} \leq h' \leq 3$
III-IV	$D' = -\frac{1}{2}h' + \frac{1}{2}$	$D' \leq -\frac{1}{2}$	$h' \geq 2$
III-VII	$D' = -\frac{1}{2}$	$D' = -\frac{1}{2}$	$2 \leq h' \leq 3$
IV-V	$D' = -\frac{1}{2}$	$D' = -\frac{1}{2}$	$1 \leq h' \leq 2$
IV-IX	$D' = -h' + \frac{1}{2}$	$D' \leq -\frac{1}{2}$	$h' \geq 1$
V-VI	$D' = -\frac{1}{4}h' - \frac{1}{4}$	$-\frac{1}{2} \leq D' \leq -\frac{1}{4}$	$0 \leq h' \leq 1$
V-VII	$D' = h' - \frac{5}{2}$	$-\frac{1}{2} \leq D' \leq 0$	$2 \leq h' \leq \frac{5}{2}$
VI-IX	$D' = -\frac{1}{2}$	$D' = -\frac{1}{2}$	$0 \leq h' \leq 1$

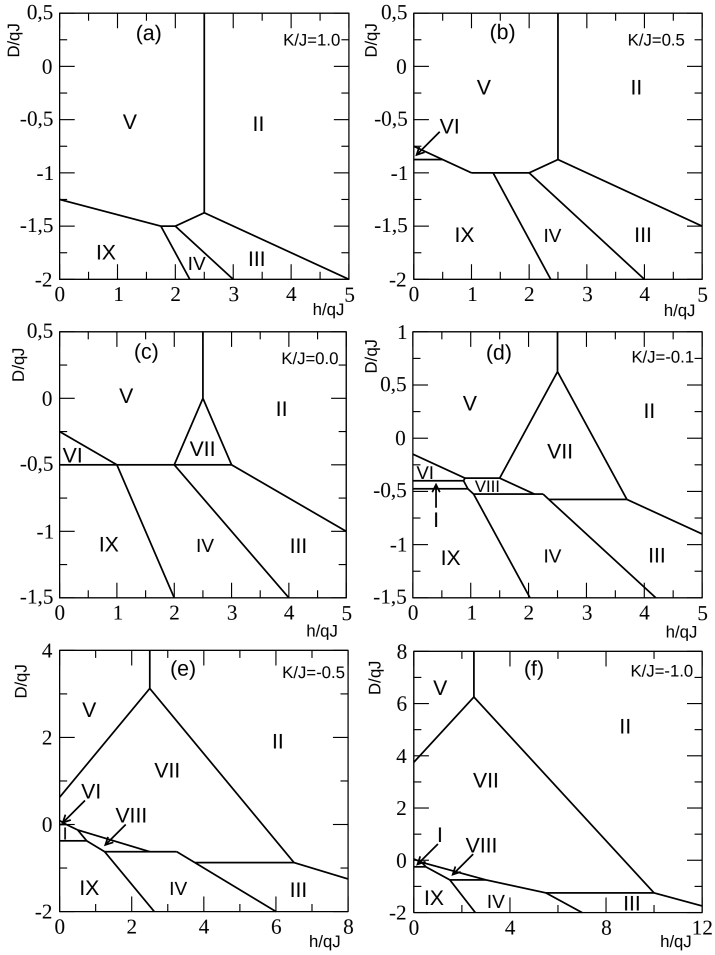

FIG. 4: Ground state phase diagrams for selected values of K/J and varying h/qJ and D/qJ. The different phases indicated with Roman numbers are explained in Table III.

Actually, the present KMC simulations are intended to evaluate the magnetization m(t) of the lattice, which may be defined as:

$$m(t) = \sum_{\overline{\sigma}} M_{\overline{\sigma}}(t).P(\overline{\sigma}, t) \tag{18}$$

Where, $P(\overline{\sigma}, t)$ stands for the probability that the system lies in configuration $\overline{\sigma}$ at real time t and $M_{\overline{\sigma}}(t)$ denotes the statistically averaged magnetization associated to configuration $\overline{\sigma}$ at time t. The time evolution of $P(\overline{\sigma}, t)$ is given by the kinetic equation:

$$\begin{aligned} dP(\overline{\sigma}, t)/dt \;=\; & -\sum_{\overline{\sigma'}} W(\overline{\sigma} \to \overline{\sigma'})P(\overline{\sigma}, t) \\ & + \sum_{\overline{\sigma'}} W(\overline{\sigma'} \to \overline{\sigma})P(\overline{\sigma'}, t) \end{aligned} \tag{19}$$

$P(\overline{\sigma}, t)$ can be calculated exactly on finite samples by the transition matrix method [28].

6. Simulation Results

We find instructive to investigate some properties of the model in the presence of a time-dependent external field acting on the system as: $h_0 sin(\omega t)$, where ω denotes the field frequency and h_0 its amplitude. Due to the multiplicity of spin states on both sub-lattices, one may expect some non-trivial behavior. First, some results by numerical simulations on the model are compared to those obtained for $q = 4$ on the Bethe lattice in the context of static field. The Bethe lattice results should cor-

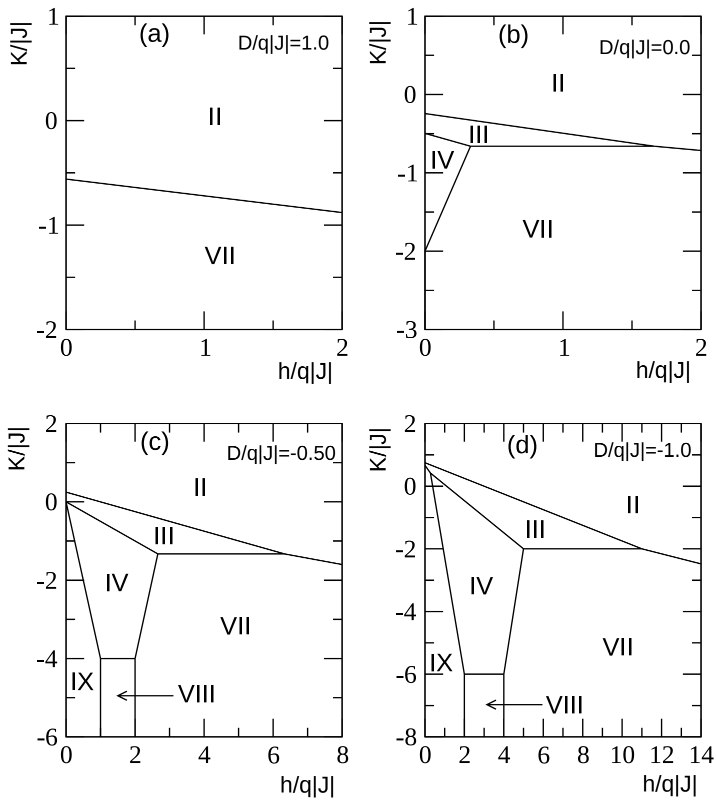

FIG. 5: Ground state phase diagrams for selected values of $D/q|J|$ and varying $h/q|J|$ and $K/|J|$. The different phases indicated with Roman numbers are explained in Table VI.

respond to exact results for an infinite square lattice within the Bethe-Peierls approximation [29]. This allows one to check the accuracy of the simulations. In Fig. 7a, full line shows the magnetization for some fixed values of the model parameters: D/J=0, K/J=0 and h/J=0, whereas signs correspond to simulation results. For these values, KMC simulations are performed on systems with linear sizes $L = 40$ and $L = 100$ with a number of updates/site, which is about 4.10^3. Results by KMC agree with those by recursion relations with a marked accuracy at low temperature. Indeed, the average steady state total magnetization m coincides at low temperature, but at high temperature where thermal fluctuations become important some discrepancy appears. The critical temperature calculated by recursion relations is $T_c \simeq 4.4J$, whereas the one given by the Binder crossing point of the cumulants associated to system sizes $L = 30; 40$ is $T_c \simeq 4.5J$ as shown in Fig. 7b. In Fig. 7c, we compare first order transition lines obtained by both methods in the case of varying values of the field strength for $D/J = -1$, $K/J = 0$. Although the two transition lines are different from each other, they again show trends that the simulation procedure is reliable. In the following, these simulations are used to study dynamical behaviors of the lattice magnetization in presence of a time-dependent field. Our aim here is not to draw a complete picture of the dynamics. Instead we would like to point out that drawing dynamic phase diagrams should only be possible within some drastic approximations. Indeed, even in the simple case of the kinetic spin-1 Blume-Capel model [20], KMC simulations show long-time limit behaviors of the magnetiza-

TABLE VI: Ground states energies of the model for $J < 0$, and $h \neq 0$; $D' = D/q|J|$, $K' = K/|J|$ and $h' = h/q|J|$.

Phase	Ground state				Energy
II	$(+1, -5/2)$	$h' > 0$	$(-1, +5/2)$	$h' < 0$	$\begin{cases} -\frac{5}{2} - \frac{29}{4}D' - \frac{25}{4}K' - \frac{7}{2}h' & \text{si } h' > 0 \\ -\frac{5}{2} - \frac{29}{4}D' - \frac{25}{4}K' + \frac{7}{2}h' & \text{si } h' < 0 \end{cases}$
III	$(+1, -3/2)$	$h' > 0$	$(-1, +3/2)$	$h' < 0$	$\begin{cases} -\frac{3}{2} - \frac{13}{4}D' - \frac{9}{4}K' - \frac{5}{2}h' & \text{si } h' > 0 \\ -\frac{3}{2} - \frac{13}{4}D' - \frac{9}{4}K' + \frac{5}{2}h' & \text{si } h' < 0 \end{cases}$
IV	$(+1, -1/2)$	$h' > 0$	$(-1, +1/2)$	$h' < 0$	$\begin{cases} -\frac{1}{2} - \frac{5}{4}D' - \frac{1}{4}K' - \frac{3}{2}h' & \text{si } h' > 0 \\ -\frac{1}{2} - \frac{5}{4}D' - \frac{1}{4}K' + \frac{3}{2}h' & \text{si } h' < 0 \end{cases}$
VII	$(0, -5/2)$	$h' > 0$	$(0, +5/2)$	$h' < 0$	$\begin{cases} -\frac{29}{4}D' - \frac{5}{2}h' & \text{si } h' > 0 \\ -\frac{29}{4}D' + \frac{5}{2}h' & \text{si } h' < 0 \end{cases}$
VIII	$(0, -3/2)$	$h' > 0$	$(0, +3/2)$	$h' < 0$	$\begin{cases} -\frac{9}{4}D' - \frac{3}{2}h' & \text{si } h' > 0 \\ -\frac{9}{4}D' + \frac{3}{2}h' & \text{si } h' < 0 \end{cases}$
IX	$(0, -1/2)$	$h' > 0$	$(0, +1/2)$	$h' < 0$	$\begin{cases} -\frac{1}{4}D' - \frac{1}{2}h' & \text{si } h' > 0 \\ -\frac{1}{4}D' + \frac{1}{2}h' & \text{si } h' < 0 \end{cases}$

TABLE VII: Coexistence curves of the model for $D = 0$; $K' = K/|J|$ and $h' = h/q|J|$. Different phases refer to Table VI.

Region	Coexistence line	K' Range	h' Range
II-III	$K' = -\frac{1}{4}h' - \frac{1}{4}$	$-\frac{2}{3} \leq K' \leq -\frac{1}{4}$	$0 \leq h' \leq \frac{5}{3}$
II-VII	$K' = -\frac{4}{25}h' - \frac{2}{5}$	$K' \leq -\frac{2}{3}$	$h' \leq \frac{5}{3}$
III-IV	$K' = -\frac{1}{2}h' - \frac{1}{2}$	$-\frac{2}{3} \leq K' \leq -\frac{1}{2}$	$0 \leq h' \leq \frac{1}{3}$
III-VII	$K' = -\frac{2}{3}$	$K' = -\frac{2}{3}$	$\frac{1}{3} \leq h' \leq \frac{5}{3}$
IV-VII	$K' = 4h' - 2$	$-2 \leq K' \leq -\frac{2}{3}$	$0 \leq h' \leq \frac{1}{3}$

tion, which strongly depend on the field frequency and amplitude [30].

Fig. 8a illustrates the behaviors of the total average magnetization of a system of size $L = 100$ for three different values of the field frequency: $\omega = 0.5$; 1.0; 10.0 rads/sec. The GS configuration used for the simulations is (+1,-5/2) at $T = 0.5J$ and field amplitude $h_0 = 0.5J$. Evidently, the long-time limit values of m(t) are not the same. This means that any physical quantity calculated, when $t \to \infty$, should depend of the field frequency. In other words, the dynamic order parameter $\overline{Q} = \frac{\omega}{2\pi} \oint m(t)dt$ often defined as one period time-averaged magnetization should depend on the field frequency ω. The stationary values of $m(t)$ seem to be an increasing function of the

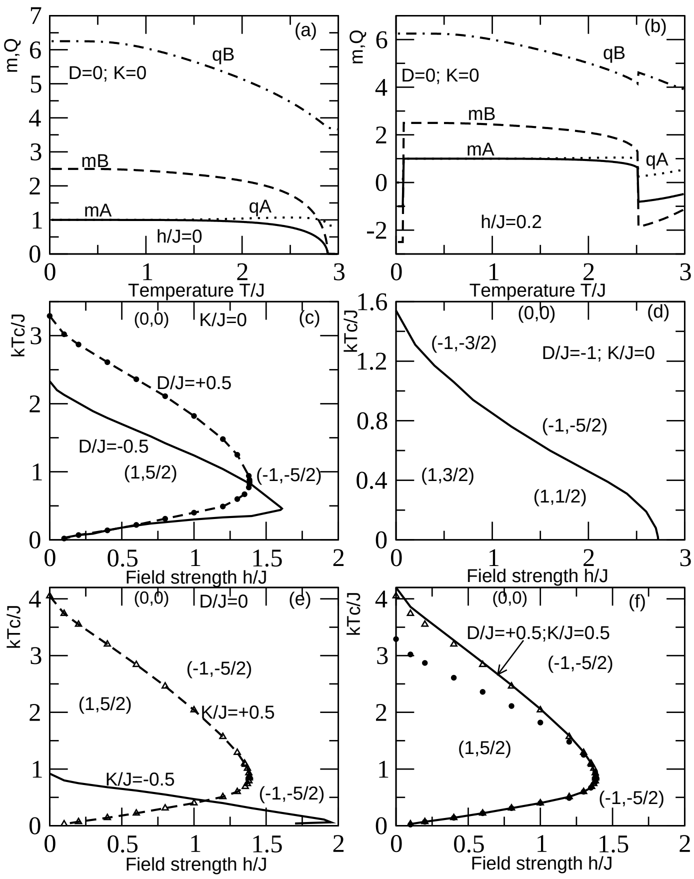

FIG. 6: Thermal behavior of sub-lattice order parameters m and Q at $h/J = 0$; $D/J = 0$; $K/J = 0$ (a) and $h/J = 0.2$ and $D/J = 0$ and $K/J = 0$ (b). In panel (a), there is a second order phase transition between a ferromagnetic and a paramagnetic phases, whereas in (b) jumps occur in the magnetization showing first order transitions between ordered phases. In panels $(c-f)$, thermal phase diagrams are presented for $D/J = \pm 0.5$ and $K/J = 0$. (c); $D/J = -1$ and $K/J = 0$ (d); $K/J = \pm 0.5$ and $D/J = 0$ (e) and $D/J = K/J = 0.5$ (f). Signs in panels (f) are simply added for comparison (see text) and refer to panels (c) and (e): triangles for $D/J = 0.5$ and $K/J = 0$ and circles for $D/J = 0$ and $K/J = 0.5$. Phases (m_A, m_B) displayed in panels (c) and (e) refer to dash transition lines with positive values of the coupling constants.

TABLE VIII: Coexistence curves of the model for $K = 0$; $D' = D/q|J|$ and $h' = h/q|J|$. Different phases refer to Table VI.

Region	Coexistence line	D' Range	h' Range
II-III	$D' = -\frac{1}{4}h' - \frac{1}{4}$	$D' \leq -\frac{1}{4}$	$h' \geq 0$
III-IV	$D' = -\frac{1}{2}h' - \frac{1}{2}$	$D' \leq -\frac{1}{2}$	$h' \geq 0$
IV-IX	$D' = -h' - \frac{1}{2}$	$D' \leq -\frac{1}{2}$	$h' \geq 0$

frequency. However other calculations show that this behavior is not so trivial but temperature-dependent (see Fig.8c). What appears evident is that with increasing temperature, the stationary values of m(t) decrease suggesting that the dynamic order parameter $\overline{Q}$ should decrease with the temperature. Other surprising results given by the simulations are displayed in Fig.8e. Actually, the time evolution should depend on initial conditions but the stationary behaviors might be the same. Panels (c) and (e) display results that contrast with this picture because the expected saturated values of m(t) or simply the expected values of $\overline{Q}$ seem to depend on the GS configurations. Hence, the

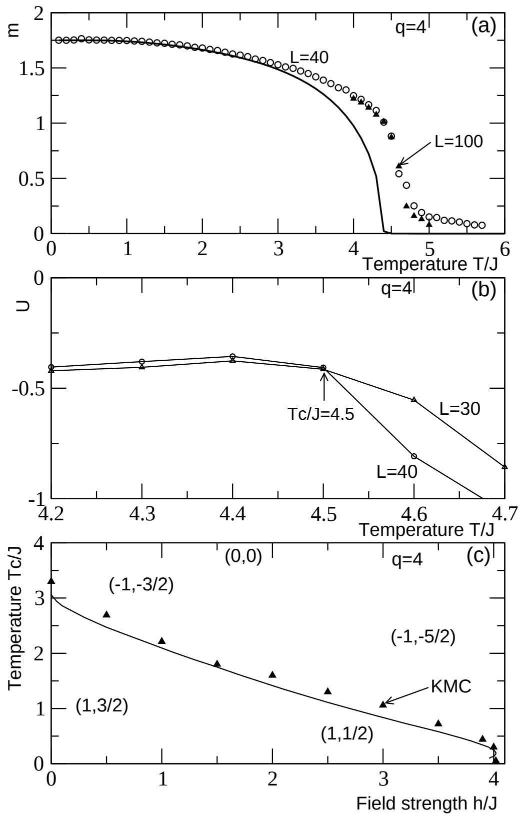

FIG. 7: Compared results by recursion relations (full line) on the Bethe lattice and KMC simulations on a square lattice (signs) of sizes $L = 100$ and $L = 40$ for a coordination number $q = 4$ (panel (a)). In panel (b), a binder crossing point of cumulants $U_L(t)$ calculated for two system sizes $L = 40$ and $L = 30$ is shown. This point indicates a transition temperature $T_c = 4.5J$, which is very close to that obtained by recursion relations. In panel (c), phase diagrams are compared by both methods in the case: $D/J = -1.0$, $K/J = 0$ and $q = 4$. Full line shows results by recursion relations, whereas signs indicate simulation results by means of cumulant calculations. Marked agreement between both transition lines appears evident.

system presents some chaotic features. In panel (b), we show the stationary behavior of m(t) for $\omega = 1.0 rads/sec$. The dynamical behavior of the system is evident. The magnetization reproduces exactly the period of the field. Maxima and minima of m(t) are slowly decaying in this region of ωt investigated but the amplitude and the period of m(t) appear somewhat constant. Calculations of energy loss that is proportional to hysteresis area can only be performed within some approximations since associated hysteresis curves should not be completely closed in such situation. In Fig. 8d,f the effect of the field amplitude on m(t) is illustrated at two field frequencies. Here again the behavior of m(t) is non-trivial. At large frequencies, stationary values of m(t) decrease with the field amplitude, whereas at low frequencies, different trends are observed.

We also checked the influence of the reduced crystal-field strength D/J on the stationary behaviors of $m(t)$ for two initial configurations: (+1, -5/2) and (+1, +5/2) at fixed values of the field frequency. The results revealed also non-trivial behaviors of m(t) and the stationary states are initial configurations dependent. One may be tempted to perform several runs and make averages over for the two quantities, the magnetization m(t) and the real evolution time t, at each update per site. This method gives good dynamical behavior of m(t) as observed in Fig. 8b in some time ranges and chaotic behavior in other ranges with some cellular structures as observed some time ago by one of the authors [31] on chaotic growing 1d-interfaces. Further investigations of the dynamics are certainly needed to substantiate information on the present model and to check whether most reported phenomena are due to the staggered nature of the external field acting on the two sub-lattices.

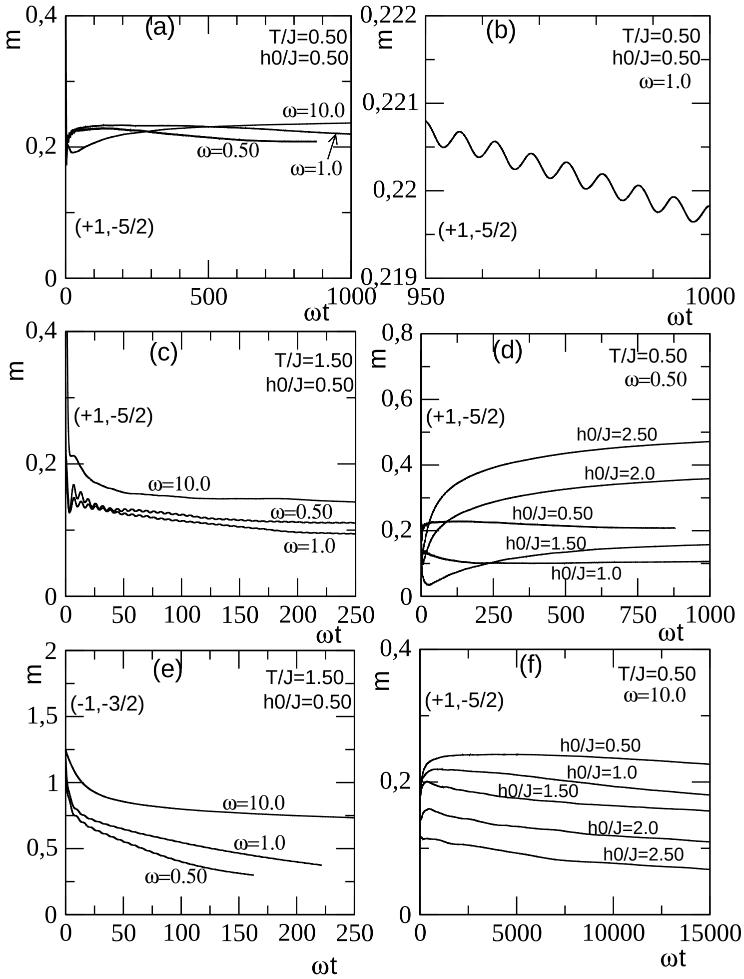

FIG. 8: Time evolution of the lattice total magnetization m(t) were obtained by KMC simulations for a system of size $L = 100$. The values of the model parameters considered are written in different panels. In panels (a), (c) and (e), the effect of the field frequency on m(t) is shown for two different GS configurations. On the contrary, in panels (d) and (f), the effect on the amplitude on the stationary behavior of m(t) is investigated for the same initial configuration. Calculations are performed for $K/J = -0.5$ and $D/J = 0$. Behaviors of m(t) with model parameters appear non-trivial.

7. Conclusion

In this work, we study a ferromagnet described by a BEG Hamiltonian that comprises an external staggered magnetic field. We extensively investigated the T=0 phase diagram of the model which appeared very rich. We defined different ground state configurations, calculated their energies and equations of coexistence lines between them. These T=0 phase diagrams may give insight on the model properties in situations where the temperature appears as a non relevant parameter and also on the low-temperature behavior of the model. Thermal behaviors of sub-lattice magnetizations have been calculated in the presence of the input field. We exclusively observed, within the domain of parameters analyzed, first order transitions between ordered phases. The paramagnetic phase (0,0) is obtained at high temperatures after crossover regions where sublattice magnetizations progressively vanish. The model is also investigated in the presence of a time-dependent sinusoidal field. Several anomalous behaviors of the stationary values of the lattice magnetization have been reported with varying model parameters. These results particularly depend on initial conditions, field amplitude and frequency.

Acknowledgments

F. H. acknowledges financial support during a visit to The Abdus Salam International Centre for Theoretical Physics (ICTP), Trieste (Italy) where some of the calculations reported in this work have been performed.

References

[1] C. Ekiz, Physica A **353**, 286 (2005).
[2] B. Deviren, M. Keskin and O. Canko, Physica A **388**, 1835 (2009).
[3] S. Maťašovská and M. Jaščur, Physica A **383**, 339 (2007).
[4] E. Albayrak and A. Yigit, Phys. Status Solidi B **244**, 748 (2007).
[5] E. Albayrak and A. Yigit, Phys. Lett. A **353**, 121 (2006).
[6] Q. Zhang, G. Wei and Y. Gu, Phys. Status Solidi B **242**, 924 (2005).
[7] R. A. Yessoufou, A. H. Amoussa and F. Hontinfinde, Cent. Eur. J. Phys. **7**, 555 (2009).
[8] N. De La Espriella and G. M. Buendìa, Physica A **389**, 2725 (2010).
[9] M. Keskin, M. Ertas and O. Canko, Phys. Scr. **79**, 025501 (2009).
[10] Z. G. Wei, W. Y. Gu and J. Liu, Phys. Rev. B **74**, 024422 (2006);
Q. Zhang, G. Wei, Z. Win and Y. Lang, J. Magn. Magn. Mater. **280**, 14 (2004).
[11] E. Albayrak and A. Yigit, Physica A **349**, 471 (2005).
[12] O. Khan, Molecular Magnetism, VCH, New york, 1993;
T. Mallah, S. Thiébaut, M. Vardegauer and P. Veillet, Science **262**, 1554 (1993);
C. Mathonière, C. J. Nutall, S. G. Carling and P. Day, Inorg. Chem. **35**, 1201 (1996).
[13] D. R. Evans and C. A. Reed, J. Am. Chem. Soc. **122**, 4460 (2000).
[14] N. A. Rakow and K. S. Suslick, Nature **406**, 710 (2000);
M. E. Kosal and K. S. Suslick, J. Solid State Chem. **152**, 87 (2000).
[15] R. A. Yessoufou, S. Bekhechi and F. Hontinfinde, Eur. Phys. J. B **81**, 137 (2011).
[16] M. Oshikawa and I. Affeck, Phys. Rev. Lett. **82**, 5136 (1999);
M. Sato and M. Oshikawa, Phys. Rev. B **69**, 054406 (2004).
[17] O. Canko and M. Keskin, Phys. Lett. A **320**, 22 (2003);
O. Canko, B. Deviren and M. Keskin, Phys. Scr. **77**, 055701 (2008).
[18] A. B. Bortz, M. H. Kalos and J. L. Lebowitz, J. Comp. Phys. **17**, 10 (1975).
[19] R. J. Glauber, J. Math. Phys. **4**, 294 (1963).
[20] S. Akkaya, B. Deviren and E. Albayrak, Physica A **390**, 3289 (2011).
[21] M. Keskin, O. Canko and U. Temizer, Phys. Rev. E **72**, 036125 (2005).
[22] M. Blume, V. J. Emery and R. B. Griffiths, Phys. Rev. A **4**, 1071 (1971).
[23] N. Goveas and G. Mukhopadhyay, Phys. Scr. **56**, 661 (1997).
[24] J. Adler, PhD thesis, University of New South Wales, 1979 (unpublished).
[25] S. W. Sides, P. A. Rikvold and M. A. Novotny, J. Appl. Phys. **83**, 6494 (1998).
[26] K. Boukheddaden, M. Nishino, S. Miyashita and F. Varret, Phys. Rev. B **72**, 0144679 (2005).
[27] F. Hontinfinde and R. Ferrando, Phys. Rev. B. **63**, 121403 (R) (2001);
U. T. Ndongmouo, F. Hontinfinde and R. Ferrando, Phys. Rev. B **72**, 115412 (2005);
A. V. Kpadonou and F. Hontinfinde, Physica A **362**, 345 (2006).
[28] F. Hontinfinde, R. Ferrando and A. C. Levi, Physica A **319**, 36 (2003).
[29] C. Domb, Adv. Phys. **9**, 208 (1960).
[30] F. Hontinfinde, unpublished.
[31] J. Krug and F. Hontinfinde, J. Phys. A: Math. Gen. **30**, 30 (1997).

Received: 22 March, 2012
Accepted: 21 August, 2012